Am J Transl Res 2025;17(2):770-790
www.ajtr.org /ISSN:1943-8141/AJTR0159165

Original Article

The role of Prolyl 3-Hydroxylase 1 (P3H1) in tumor development and prognosis: a pan-cancer analysis with validation in colonic adenocarcinoma

Yanqin Chen[1], Moazzam Ali[2], Muhammad Bilal Tayyab[3], Muhammad Majid Nazir[4], Muhammad Umar[5], Salman Khan[6], Danyah Mohamed Ismail[7], Mostafa A Abdel-Maksoud[8], Hossam Ebaid[9], Abdulaziz Alamri[10], Saeedah Almutairi[8], Taghreed N Almanaa[8], Bushra Hafeez Kiani[11]

[1]Nanjing Drum Tower Hospital, Nanjing 210000, Jiangsu, China; [2]Department of Gastroenterology, Hayatabad Medical Complex Peshawar, Peshawar 25120, Khyber Pakhtunkhwa, Pakistan; [3]Institute of Drug Discovery and Development, Zhengzhou University, Zhengzhou 450001, Henan, China; [4]Department of Medicine, Bedford Hospital, General Medicine, Bedford MK42 9DJ, UK; [5]Department of Neurosurgery, Allied Hospital Faisalabad, Faisalabad 37521, Punjab, Pakistan; [6]DHQ Teaching Hospital, GMC, Dikah, Abbottabad 22010, Khyber Pakhtunkhwa, Pakistan; [7]Indira Gandhi Medical College and Research Institute Puducherry, India; [8]Department of Botany and Microbiology, College of Science, King Saud University, Riyadh 11451, Saudi Arabia; [9]Department of Zoology, College of Science, King Saud University, P.O. Box 2455, Riyadh 11451, Saudi Arabia; [10]Department of Biochemistry, College of Science, King Saud University, P.O. Box 2455, Riyadh 11451, Saudi Arabia; [11]Department of Biology and Biotechnology, Worcester Polytechnic Institute, Worcester, Massachuesetts 01609, USA

Received July 13, 2024; Accepted December 16, 2024; Epub February 15, 2025; Published February 28, 2025

Abstract: Background: Cancer is a multifaceted disease characterized by unregulated cell proliferation, evasion of apoptosis, and metastasis. Recent studies have highlighted the importance of extracellular matrix remodeling and post-translational modifications in tumorigenesis. Prolyl 3-hydroxylase 1 (P3H1), an enzyme involved in collagen hydroxylation, has gained attention for its role in cancer progression. Methods: This study investigates P3H1 expression, prognostic value, and functional relevance across multiple human cancers using a combination of bioinformatic and experimental approaches. Results: Using The Cancer Genome Atlas (TCGA) data from TIMER2.0 and UALCAN databases, we observed a significant upregulation of P3H1 mRNA and protein in various cancers. Prognostic analysis using GEPIA2 and KM plotter revealed that high P3H1 expression correlates with poorer overall survival in colon adenocarcinoma (COAD), kidney renal clear cell carcinoma (KIRC), and liver hepatocellular carcinoma (LIHC). Further, genetic and promoter methylation analyses showed low mutation frequencies and reduced methylation of P3H1 in specific cancer types. Functional and pathway enrichment analyses indicated that P3H1 is involved in collagen formation, endoplasmic reticulum activity, and pathways such as ECM-receptor interaction and PI3K-Akt signaling. Validation by enzyme linked immunosorbent assay in COAD patient serum samples demonstrated significantly elevated P3H1 levels compared to healthy controls, with an AUC approaching 1.0 by receiver operating characteristic (ROC) curve analysis. This suggests its potential as a diagnostic biomarker. Additionally, functional experiments were conducted in COAD cells to assess P3H1's role in tumorigenesis. Knockdown of P3H1 in HCT116 cells resulted in a significant reduction in cell proliferation, colony formation, and migratory abilities of these cells. Conclusion: These findings emphasize P3H1's relevance in COAD, KIRC, and LIHC pathogenesis and possible utility in clinical diagnosis.

Keywords: P3H1, pan-cancer, treatment, diagnosis, prognosis

Introduction

Cancer remains one of the leading causes of mortality worldwide, with an estimated 19.3 million new cases and 10 million cancer-related deaths [1-4]. The global burden of cancer continues to rise due to factors such as aging population, environmental exposure, and lifestyle changes [1, 5]. Common malignancies include lung, breast, colorectal, prostatic, and liver cancers, each with distinct etiology and clinical behavior [6-10]. Despite advancements in diag-

https://doi.org/10.62347/SUVC1606

nostics and therapy, many cancers still have poor prognosis due to late detection, aggressive progression, and resistance to conventional treatment [11-13]. Therefore, there is an urgent need for identifying novel biomarkers and therapeutic targets that can enhance early diagnosis and improve patient outcome. In this context, pan-cancer analysis has emerged as a powerful approach to identify genes or pathways that are involved in tumorigenesis across multiple cancer types, providing broader insight into cancer biology [14, 15]. This type of analysis allows for the detection of common molecular alterations that may serve as key drivers of malignancy, as well as the discovery of cancer-specific biomarkers that may inform targeted treatment [16].

Prolyl 3-hydroxylase 1 (P3H1) is an enzyme primarily involved in collagen biosynthesis, contributing to the hydroxylation of proline residues in collagen [17, 18]. Alterations in collagen metabolism are increasingly recognized as key components in tumor microenvironment remodeling, invasion, and metastasis [19, 20]. Though historically studied for its role in connective tissue diseases, recent research has begun to explore the involvement of P3H1 in cancer progression [21]. Emerging evidence has linked dysregulated P3H1 expression to various cancer types, including breast, lung, and head and neck cancers [22]. For instance, studies have demonstrated overexpression of P3H1 in breast cancer, where it was associated with increased tumor invasiveness and poor clinical outcome [23, 24]. In lung cancer, P3H1 was found to promote tumor growth by modulating extracellular matrix remodeling and interacting with oncogenic signaling pathways [25, 26]. Similarly, in head and neck cancer, high P3H1 expression correlated with advanced disease stage and reduced overall survival, suggesting its use as a prognostic marker [24]. Despite these findings, the pan-cancer implications of P3H1, including its expression patterns and mechanistic role across different cancer types, remain largely unexplored.

In this study, we performed a comprehensive pan-cancer analysis of P3H1, combining *in silico* and *in vitro* approaches to elucidate its expression pattern, functional role, and use as a therapeutic target across various cancers. Using publicly available genomic databases, P3H1 expression levels of multiple tumor types were compared to normal tissue counterparts to identify significant alterations. Furthermore, we conducted detailed bioinformatic analyses, including correlation with clinical outcome and survival, to determine the prognostic significance of P3H1 in different cancers. In parallel, we employed *in vitro* experiments using various cancer cell lines to investigate the functional implications of P3H1 expression. Ultimately, this research aims to pave the way for further investigation into P3H1 as a candidate for therapeutic intervention in oncology.

Methods

Sample collection

A total of 60 patients diagnosed with colon adenocarcinoma (COAD) and 30 healthy control subjects were enrolled in this study from Shoukat Khanum Memorial Cancer Hospital and Research Centre, Karachi, Pakistan, between July 1 and December 31, 2022. All participants provided written informed consent prior to their inclusion in the study, ensuring that they were fully aware of the study objectives and procedures. Venous blood samples were collected from each individual following standard phlebotomy protocols under sterile conditions. Blood samples were obtained in the morning, after participants had fasted overnight, to minimize variability' in serum biomarkers. The serum was separated through centrifugation at 3,000 rpm for 10 minutes and stored at -80°C until further analysis. All procedures adhered to the ethical guidelines and were approved by the hospital's Institutional Review Board (IRB).

Gene expression analysis using The Cancer Genome Atlas (TCGA) datasets

TIMER2.0 (http://timer.cistrome.org/) and UALCAN (https://ualcan.path.uab.edu/) are powerful web tools used for cancer research and genomic data analysis. TIMER2.0 allows researchers to explore gene expression and tumor immune infiltration across multiple cancer types by analyzing RNA-seq data [27]. It provides insight into immune cell types in the tumor microenvironment and their correlation with gene expression. UALCAN is used for interactive analysis of RNA-seq expression data from the TCGA projects, offering customizable options for differential expression, survival

analysis, and correlation studies in various cancers [28]. In this work, both TIMER2.0 and UALCAN were used for the pan-cancer expression analysis of P3H1.

Survival analysis of P3H1

GEPIA2 (http://gepia2.cancer-pku.cn/) and KM Plotter (https://kmplot.com/analysis/) are widely used bioinformatic tools for cancer research. GEPIA2 allows users to analyze RNA-seq data from TCGA and GTEx, offering features like differential expression analysis, survival analysis, and gene correlation studies across various cancer types [29]. Kaplan-Meier Plotter (KM) focuses on survival analysis, utilizing gene expression data to generate Kaplan-Meier survival curves [30]. It helps assess the effect of specific genes on patient survival in different cancers, providing insight into prognostic biomarkers. Herein, we used GEPIA2 and KM plotter web sources to conduct pan-cancer survival analysis on P3H1.

Correlation of P3H1 with clinical variables of cancer patients

UALCAN (https://ualcan.path.uab.edu/) is a comprehensive web resource for analyzing cancer transcriptome data, offering user-friendly tools for exploring gene expression, survival analysis, and clinical data from TCGA and MET500 databases [28]. UALCAN was used to evaluate the correlation of P3H1 with clinical variables of cancer patients.

Genetic mutation and promoter methylation analysis of P3H1

OncoDB (https://oncodb.org/) is a user-friendly database designed for cancer genomics research [31]. It integrates multi-omics data, including gene expression, mutation, copy number variation, and clinical information from various cancer types. OncoDB enables researchers to explore molecular alterations, perform survival analysis, and identify potential biomarkers. This work used the OncoDB database to perform genetic mutation and promoter methylation analysis of P3H1 across the TCGA datasets.

Correlations of P3H1 with diverse functional state of the tumor

CancerSEA (http://biocc.hrbmu.edu.cn/CancerSEA/) is a specialized database that focuses on single-cell sequencing data to explore cancer cell functional state [32]. It provides insight into the diverse roles of genes across various cancer types, linking gene expression to cellular activities like proliferation, metastasis, and immune response, enabling researchers to investigate cancer heterogeneity at the single-cell level. We used CancerSEA database in this work to explore correlations of P3H1 with diverse functional states of the tumor.

microRNA (miRNA) prediction and expression analysis

TargetScan (https://www.targetscan.org/vert_80/) is a bioinformatic tool designed to predict miRNA target genes in various species, including humans [33]. It uses sequence-based algorithms to identify conserved miRNA binding sites in the 3' untranslated regions (3'UTR) of mRNA. TargetScan helps researchers explore miRNA-gene interactions, offering insight into gene regulation, post-transcriptional control, and the functional impact of miRNA on biological pathways and diseases. Herein, TargetScan was used to predict the P3H1 expression effect of regulatory miRNA.

Next, expression profiling of the predicted miRNA (has-mir-10a-5p) was done in the blood samples 60 COAD and 30 normal individuals using reverse transcription quantitative polymerase chain reaction (RT-qPCR). Total RNA, including small RNAs, was extracted from the blood using the miRNeasy Mini Kit (ThermoFisher, Cat. No. 217004), following the manufacturer's protocol. RNA concentration and purity were assessed using a NanoDrop spectrophotometer. For miRNA-specific reverse transcription, total RNA was reverse transcribed using the TaqMan™ Advanced miRNA cDNA Synthesis Kit (ThermoFisher, Cat. No. A28007). The reaction was performed according to the kit's guidelines to convert miRNA, including hsa-miR-10a-5p, into complementary DNA (cDNA).

The cDNA was then subjected to quantitative real-time PCR (RT-qPCR) using the TaqMan™ Fast Advanced Master Mix (ThermoFisher, Cat. No. 4444557) and specific TaqMan™ miRNA Assay for hsa-miR-10a-5p (ThermoFisher, Cat. No. 4427975). U6 small nuclear RNA was used as an internal control for normalization. The RT-qPCR reaction was carried out in a 96-well plate using the QuantStudio™ 3 Real-Time PCR

System (ThermoFisher, Cat. No. A28136). The relative expression levels of hsa-miR-10a-5p were calculated using the $2^{-\Delta\Delta Ct}$ method, comparing COAD patient samples to normal controls.

Immune infiltration and drug sensitivity analysis of P3H1

GSCA (Gene Set Cancer Analysis, https://guolab.wchscu.cn/GSCA) is a comprehensive database designed for multi-omics data analysis in cancer research [34]. This web source integrates data on gene mutations, expression, methylation, and copy number variations, providing a tool for functional enrichment, pathway analysis, and immune infiltration studies. In the current work, GSCA was used for immune infiltration and drug sensitivity analysis of P3H1.

Protein-protein interaction (PPI) network construction and gene enrichment analysis

STRING (https://string-db.org/) database is a comprehensive database focused on PPIs [35]. It integrates data from various sources, including experimental studies, computational predictions, and curated databases, to provide a comprehensive view of protein interactions across different organisms. Using this web source, a PPI network of P3H1 was constructed. The PPI network was then subjected to gene enrichment analysis using DAVID tool. DAVID is a bioinformatic tool designed to provide functional annotation and analysis of gene lists [36]. It integrates multiple databases to offer insight into biological processes, molecular functions, and cellular components associated with genes of interest. Users can upload gene lists from various sources, and DAVID performs enrichment analysis to identify over-represented biological themes and pathways.

Enzyme Linked Immunosorbent Assay (ELISA)

The concentration of P3H1 in serum was measured using an ELISA kit from Cloud-Clone Corp., United States of America (USA), following the manufacturer's instructions. A 96-well microtiter plate was coated with the capture antibody and incubated overnight at 4°C. After washing with buffer, blocking buffer was added for 1 hour at room temperature to prevent nonspecific binding. Serum samples (1:2 dilution) were added in duplicate, along with standards to create a standard curve of P3H1 concentrations. The plate was incubated for 2 hours at room temperature, followed by five washes and the addition of a detection antibody, which incubated for another hour. After washing, a substrate solution was added and incubated in the dark for color development. A stop solution was added to halt the reaction, and optical density (OD) was measured at 450 nm using a microplate reader. P3H1 concentrations in serum samples were calculated from a standard curve of OD values.

Cell culture

The HCT116 human colorectal carcinoma cell line was obtained from the American Type Culture Collection (ATCC, catalog number CCL-247). Cells were cultured in McCoy's 5A medium (ATCC-formulated, modified with 10% fetal bovine serum [FBS] and 1% penicillin-streptomycin) to maintain optimal growth conditions. Cells were incubated at 37°C in a humidified atmosphere with 5% CO_2. Cells were passaged at approximately 70-80% confluency by detaching with 0.25% trypsin-EDTA solution and reseeding at a 1:4 to 1:6 ratio. Cell viability and density were assessed using trypan blue exclusion, and cultures were regularly monitored to ensure mycoplasma-free status.

P3H1 knockdown

P3H1 gene knockdown in HCT116 cells was achieved using Thermo Fisher Silencer™ Select siRNA targeting P3H1 (Catalog #AM16708). Cells were transfected with siRNA using Lipofectamine™ RNAiMAX Transfection Reagent (Thermo Fisher, Catalog #13778150) following the manufacturer's instructions. Briefly, cells were seeded in 6-well plates and allowed to reach 60-70% confluency. siRNA and Lipofectamine™ RNAiMAX were diluted in Opti-MEM™ Reduced Serum Medium (Catalog #31985062), mixed, and added to the cells for 24-48 hours. After transfection, cells were harvested for RNA extraction and further assays.

Reverse transcription quantitative polymerase chain reaction (RT-qPCR) for knockdown efficiency

Total RNA was extracted using the PureLink™ RNA Mini Kit (Thermo Fisher, Catalog #121-83018A). cDNA synthesis was performed with

the High-Capacity cDNA Reverse Transcription Kit (Thermo Fisher, Catalog #4368814). Real-time PCR was conducted using PowerUp™ SYBR™ Green Master Mix (Thermo Fisher, Catalog #A25742) on a real-time PCR system. GAPDH was used as a housekeeping gene. Relative quantification of P3H1 expression was calculated using the $2^{-\Delta\Delta Ct}$ method to assess knockdown efficiency. Following primers were used for the amplification of GAPDH and P3H1.

GAPDH-F 5'-ACCCACTCCTCCACCTTTGAC-3', GAPDH-R 5'-CTGTTGCTGTAGCCAAATTCG-3'; P3H1-F 5'-CTGCAGCACACACCTTCTTC-3', P3H1-R 5'-ACAGCTTCCTGTGGCTGTTC-3'.

Cell proliferation assay

Cell proliferation was assessed using the CellTiter 96® AQueous One Solution Cell Proliferation Assay (MTS assay, Fisher Scientific, Catalog #G3580). Cells were seeded in 96-well plates at a density of 2,000 cells per well and allowed to attach overnight. The MTS reagent was added to each well and incubated for 1-4 hours at 37°C. Absorbance was measured at 490 nm using a microplate reader, and the data was analyzed to assess cell viability.

Colony formation assay

To evaluate the effect of P3H1 knockdown on colony formation, Gibco™ Cell Culture Freezing Media (Thermo Fisher, Catalog #12648010) was used to prepare single-cell suspensions. Approximately 500 cells were plated in 6-well plates and incubated for 10-14 days in complete McCoy's 5A medium. Colonies were then fixed with methanol, stained with Crystal Violet Staining Solution (Thermo Fisher, Catalog #R40052), and counted under a microscope.

Wound healing assay

Cells were cultured in 6-well plates until reaching 100% confluency. A sterile 200 µL pipette tip was used to create a uniform scratch across the monolayer. The cells were then washed twice with phosphate-buffered saline (PBS) to remove debris and incubated in serum-free McCoy's 5A medium. Images were captured at 0 and 24 hours post-scratch using a phase-contrast microscope to measure wound closure.

Statistical analysis

Data were analyzed using IBM SPSS Statistical software for Windows, version 22.0 (IBM Corporation, Armonk, NY, USA) and GraphPad software (GraphPad Software, Inc., La Jolla, CA, USA). Results from the ELISA were statistically analyzed using an unpaired t-test. Additionally, the area under the curve (AUC) was calculated to evaluate the diagnostic performance of P3H1 concentration in distinguishing between COAD samples and normal controls. *P < 0.05, **P < 0.01, and ***P < 0.001 were considered significant.

Results

P3H1 expression across multiple human cancers

To investigate the differential expression of P3H1 in human cancers, we analyzed its expression levels in the TCGA dataset using TIMER2.0 and UALCAN databases. As shown in **Figure 1A** and **1B**, P3H1 mRNA expression was significantly upregulated in several cancer types, including BLCA, BRCA, CHOL, COAD, ESCA, GBM, HNSC, KIRC, KIRP, LIHC, LUAD, LUSC, PRAD, READ, STAD, THCA, and UCEC. However, no statistically significant differences in P3H1 expression were observed in CESC, PAAD, PCPG, and SKCM. Additionally, P3H1 protein levels were found to be elevated in BRCA, COAD, OV, KIRC, UCEC, LUAD, PAAD, HNSC, GBM, and LIHC (**Figure 1C**).

Prognostic value of P3H1 across multiple human cancers

The prognostic significance of P3H1 across various human cancers was assessed using GEPIA2 and the KM plotter tool. **Figure 2A** displays a heatmap of survival outcomes in different cancers based on P3H1 expression from TCGA data by GEPIA2. COAD, KIRC, and LIHC notably exhibited higher hazard ratios (HRs), indicating a poorer prognosis with elevated P3H1 expression (**Figure 2A**). **Figure 2B** and **2C** show KM plots from GEPIA2 and KM plotter for COAD, KIRC, and LIHC, where high P3H1 expression is consistently associated with significantly worse overall survival (OS), highlighting an increased mortality risk in patients with elevated P3H1 levels.

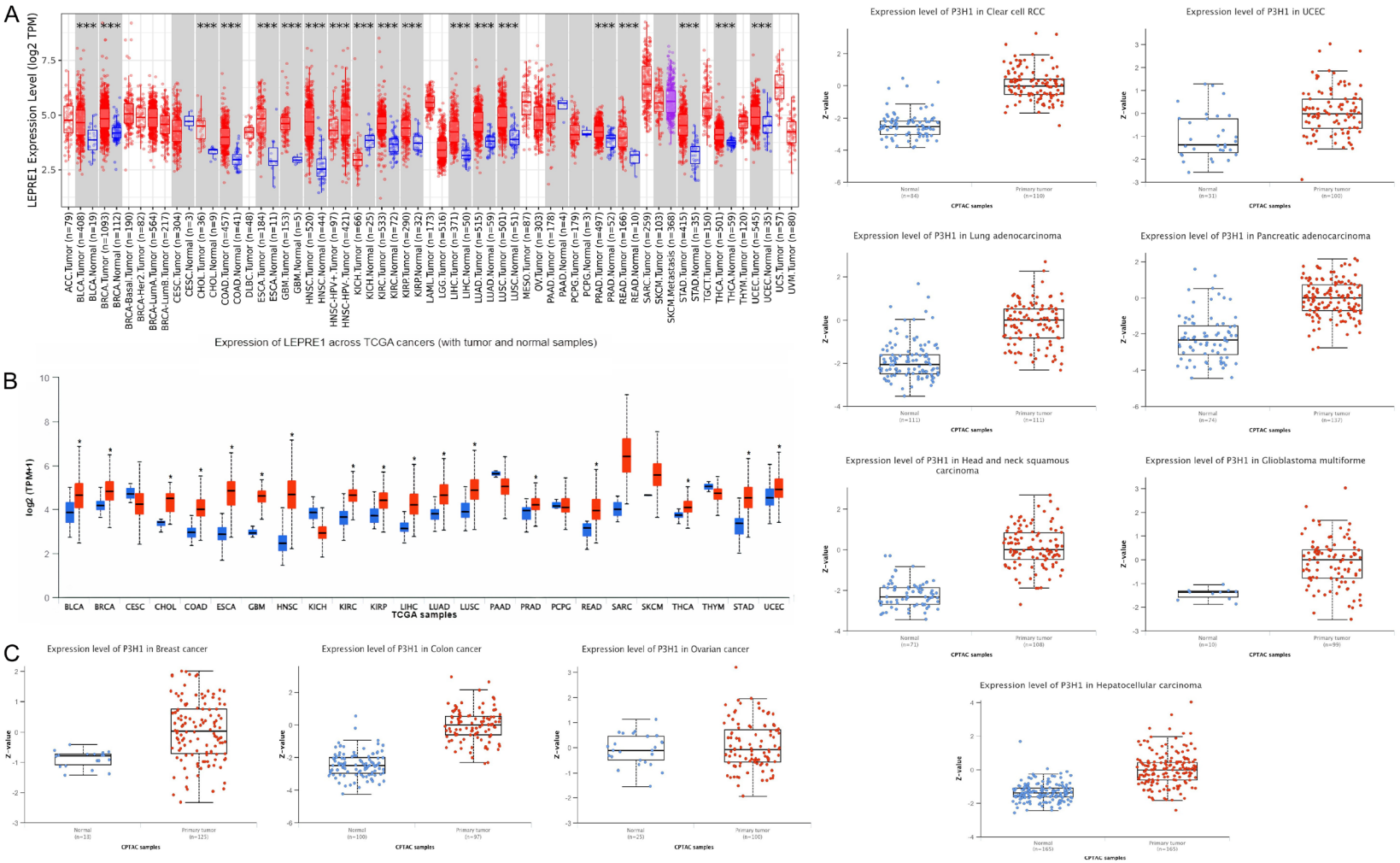

Figure 1. Pan-cancer expression analysis of Prolyl 3-Hydroxylase 1 (P3H1) using TIMER2.0 and UALCAN databases. A. The mRNA expression levels of LEPRE1 (Leprecan-like Protein 1, also known as P3H1) across various tumor types compared to normal tissue samples were analyzed using TIMER2.0. B. Pan-cancer mRNA expression analysis of LEPRE1 (P3H1) across various cancers and normal samples using UALCAN. C. Differential protein expression of P3H1 in various cancers using UALCAN. *P < 0.05 and ***P < 0.001.

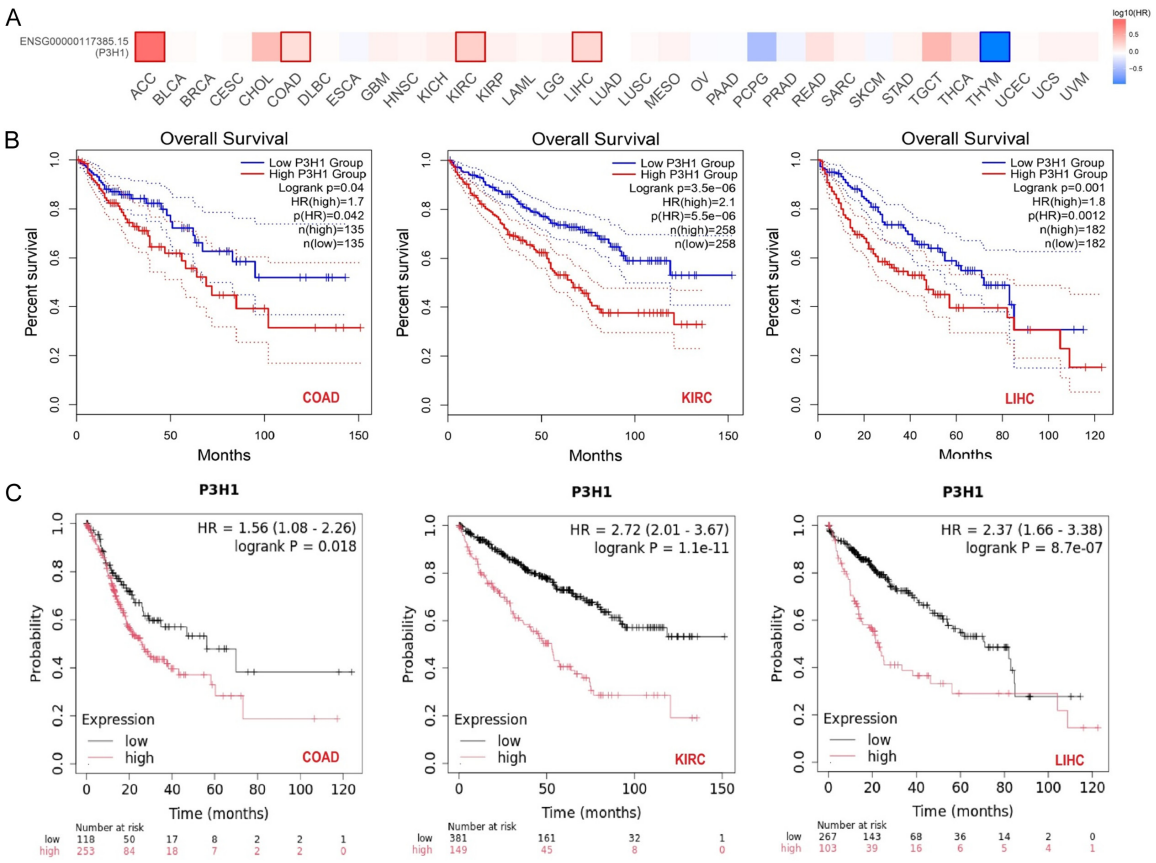

Figure 2. Prognostic significance of Prolyl 3-Hydroxylase 1 (P3H1) expression with overall survival in multiple cancer types. A. Survival map generated from GEPIA2 showing the hazard ratio (HR) of P3H1 across various cancers. B. Kaplan-Meier overall survival curves for high and low P3H1 expression groups in colon adenocarcinoma (COAD), kidney renal clear cell carcinoma (KIRC), and liver hepatocellular carcinoma (LIHC), using GEPIA2. C. Survival curves from the KM Plotter for COAD, KIRC, and LIHC. Patients are grouped into high and low P3H1 expression categories, with statistical data indicating that high P3H1 expression was significantly correlated with poor prognosis in all three cancer types. P < 0.05.

Correlation of P3H1 expression with clinical variables

Correlations of P3H1 expression with different clinical variables of COAD, KIRC, and LIHC were evaluated using UALCAN database. In **Figure 3A**, left plot shows that the P3H1 expression was significantly (p-value < 0.05) upregulated in stages 1 to 4 of COAD compared to normal tissue, with the highest expression in stages 2 and 4. The middle plot reveals a significantly (p-value < 0.05) higher expression of P3H1 in African-American, Caucasian, and Asian COAD patient groups (**Figure 3A**). In terms of gender (right plot), both females and male COAD patients exhibited significantly (p-value < 0.05) higher P3H1 expression compared to normal tissues (**Figure 3A**). **Figure 3B** shows a similar trend, with P3H1 expression significantly (p-value < 0.05) increased in all KIRC 1 to 4 cancer stages compared to normal tissues (**Figure 3B**). When stratified by race, P3H1 expression was notably (p-value < 0.05) higher in African-American and other racial groups of KIRC patients relative to normal controls (**Figure 3B**). Additionally, both male and female had a significantly (p-value < 0.05) higher expression of P3H1 than normal tissues, as seen in the gender-specific plot (**Figure 3B**). **Figure 3C** reveals significantly (p-value < 0.05) elevated P3H1 expression across all LIHC stages (1 to 4) compared to normal samples (**Figure 3C**). Regarding racial differences, P3H1 expression was significantly (p-value < 0.05) high in African-American, Caucasian, and Asian LIHC patients as compared to the normal controls (**Figure 3C**). In the gender-based analysis, both males and females again exhibited significantly (p-value < 0.05)

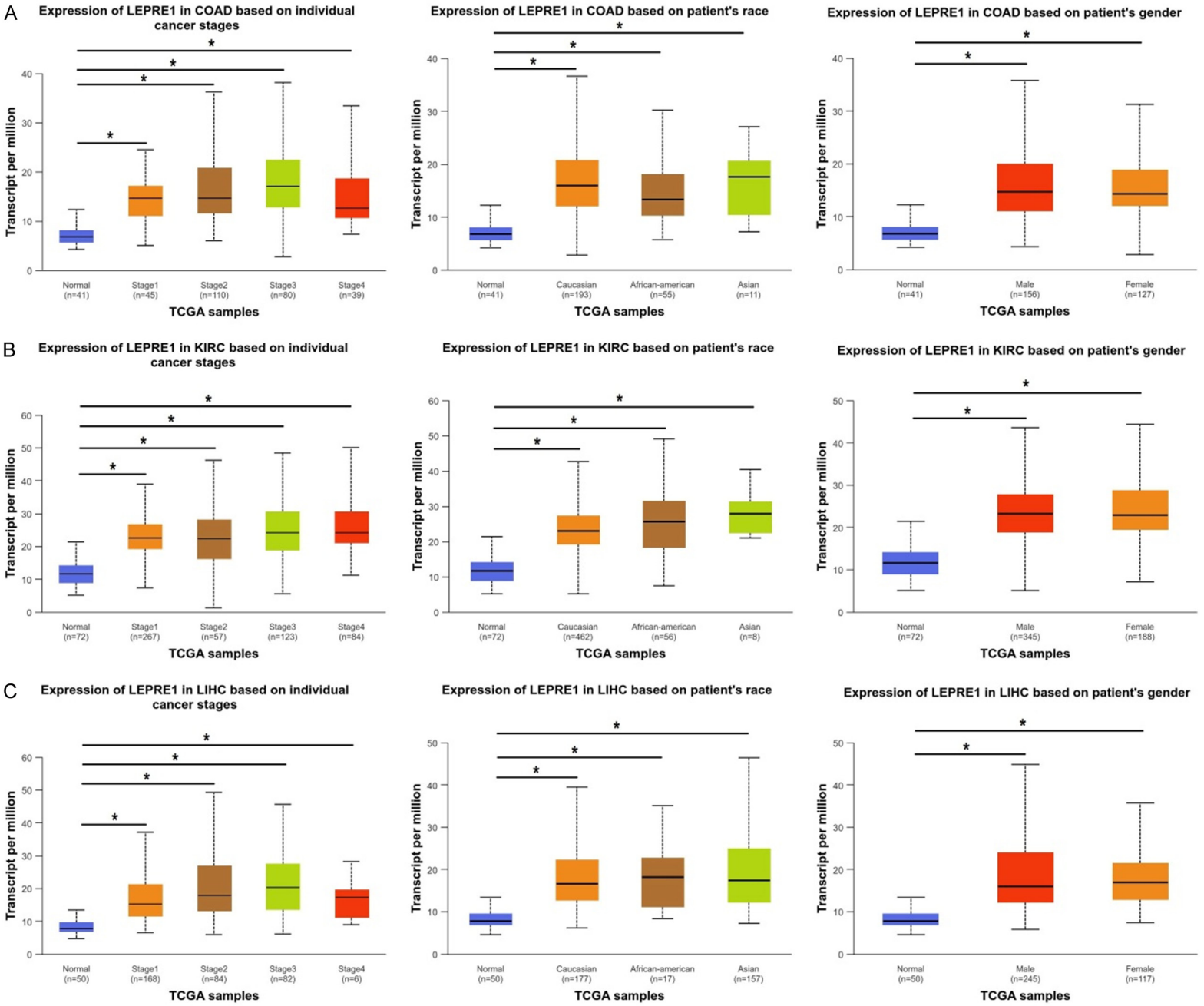
A
Expression of LEPRE1 in COAD based on individual cancer stages
Transcript per million
Normal (n=41)
Stage1 (n=45)
Stage2 (n=110)
Stage3 (n=80)
Stage4 (n=39)
TCGA samples
Expression of LEPRE1 in COAD based on patient's race
Normal (n=41)
Caucasian (n=193)
African-american (n=55)
Asian (n=11)
TCGA samples
Expression of LEPRE1 in COAD based on patient's gender
Normal (n=41)
Male (n=156)
Female (n=127)
TCGA samples
B
Expression of LEPRE1 in KIRC based on individual cancer stages
Normal (n=72)
Stage1 (n=267)
Stage2 (n=57)
Stage3 (n=123)
Stage4 (n=84)
TCGA samples
Expression of LEPRE1 in KIRC based on patient's race
Normal (n=72)
Caucasian (n=462)
African-american (n=56)
Asian (n=8)
TCGA samples
Expression of LEPRE1 in KIRC based on patient's gender
Normal (n=72)
Male (n=345)
Female (n=188)
TCGA samples
C
Expression of LEPRE1 in LIHC based on individual cancer stages
Normal (n=50)
Stage1 (n=168)
Stage2 (n=84)
Stage3 (n=82)
Stage4 (n=6)
TCGA samples
Expression of LEPRE1 in LIHC based on patient's race
Normal (n=50)
Caucasian (n=177)
African-american (n=17)
Asian (n=157)
TCGA samples
Expression of LEPRE1 in LIHC based on patient's gender
Normal (n=50)
Male (n=245)
Female (n=117)
TCGA samples

Figure 3. Correlation of LEPRE1 (Leprecan-like Protein 1, also known as P3H1) expression with clinical variables in colon adenocarcinoma (COAD), kidney renal clear cell carcinoma (KIRC), and liver hepatocellular carcinoma (LIHC) using the UALCAN database. A. P3H1 expression in COAD based on cancer stage, patient race, and gender. B. P3H1 expression in KIRC based on cancer stage, patient race, and gender. C. P3H1 expression in LIHC based on cancer stage, patient race, and gender. *P < 0.05.

higher P3H1 expression compared to normal tissues (**Figure 3C**).

Genetic mutations and promoter methylation analysis of P3H1

Genetic mutations and promoter methylation analysis of P3H1 was conducted using OncoDB database. **Figure 4A** and **4B** summarize P3H1 mutation subtypes in COAD, KIRC, and LIHC. In COAD, various mutation types were observed, including missense mutations, intron mutations, silent mutations, and nonsense mutations, with a mutation frequency of 2.7% across 433 patients (**Figure 4A**, **4B**). In KIRC, a single splice site mutation was identified with a mutation frequency of 0.3% in 287 patients (**Figure 4A**, **4B**). Across LIHC, two missense mutations were detected, corresponding to a mutation frequency of 0.5% in 373 patients (**Figure 4A**, **4B**). These findings indicate that P3H1 mutations occur at low frequencies in these cancers. **Figure 4C** and **4D** present the results of promoter methylation analysis of P3H1 across COAD, KIRC, and LIHC. The analysis reveals differential methylation patterns between cancer and normal samples, with most cancer samples in COAD and KIRC patient groups exhibiting lower levels of methylation compared to normal tissues (**Figure 4C**, **4D**). Meanwhile, in the LIHC patient group, no significant difference in promoter methylation level of P3H1 was noted relative to control samples (**Figure 4C**, **4D**).

Correlation of P3H1 with diverse functional states, miRNA prediction, and validation analysis

Initially, the correlations of P3H1 expression with diverse clinical states of COAD, KIRC, and LIHC were analyzed using CancerSEA database. In **Figure 5A** and **5B**, P3H1 expression was correlated (negatively and positively) with different stats, including apoptosis, EMT (epithelial-to-mesenchymal transition), DNA damage repair, and quiescence in these cancers (**Figure 5A**, **5B**). Furthermore, **Figure 5C** shows the TargetScan-based predicted miRNA targeting P3H1, highlighting evolutionary conservation across various species. Results of this analysis suggested that miR-10a-5p was highly conserved in humans and other organisms, supporting a regulatory role of this miRNA in P3H1 expression. Furthermore, **Figure 5D** provides the validation of hsa-miR-10a-5p expression in COAD (n = 60) vs normal (n = 30) blood samples using RT-qPCR. The box plot shows significantly (p-value < 0.01) lower expression of hsa-miR-10a-5p in COAD blood samples compared to normal samples. This implies that downregulation of miR-10a-5p may contribute to the dysregulation of P3H1 in COAD, potentially influencing cancer progression.

Immune infiltration and drug sensitivity analysis of P3H1

The correlations of P3H1 expression with immune infiltrates and drug sensitivity were evaluated using the GSCA database. In COAD, P3H1 expression showed significant negative correlations with certain immune cell types, particularly Th17 and Tcm (central memory T cells) (**Figure 6A**). This suggests that higher expression of P3H1 is associated with reduced infiltration of these specific immune cells in COAD. For KIRC, P3H1 expression exhibited significant negative correlations with immune cell types like Th17, Tcm, and Tfh (follicular helper T cells) (**Figure 6B**). This implies that in KIRC, higher P3H1 expression was linked with decreased infiltration of these immune cells. In LIHC, P3H1 expression had significant negative correlations with Tfh, Th17, Tcm, and Effector Treg cells (**Figure 6C**). This indicates that elevated P3H1 expression in LIHC was also associated with a reduction in the presence of these immune cell types. Furthermore, **Figure 6D** provides an analysis of the correlation between P3H1 expression and drug sensitivity, using the Genomics of Drug Sensitivity in Cancer (GDSC) database through GSCA. The correlation analysis showed that P3H1 expression was moderately correlated with the resistance to specific drugs like axitinib, sorafenib, and dasatinib, with positive correlations (**Figure 6D**). These drugs are typically used in cancer therapy, sug-

A

P3H1 mutation subtypes in COAD by combined DNA-seq and RNA-seq analyses

Gene	Cancer type	Mutation type	num of patients with mutation	mutation frequency	Total patients
P3H1	COAD	Missense_Mutation	5	1.2%	433
		Intron	3	0.7%	
		Silent	3	0.7%	
		Nonsense_Mutation	1	0.2%	
		Frame_Shift_Del	1	0.2%	

P3H1 mutation subtypes in KIRP by combined DNA-seq and RNA-seq analyses

Gene	Cancer type	Mutation type	num of patients with mutation	mutation frequency	Total patients
P3H1	KIRC	Splice_Site	1	0.3%	287

P3H1 mutation subtypes in LIHC by combined DNA-seq and RNA-seq analyses

Gene	Cancer type	Mutation type	num of patients with mutation	mutation frequency	Total patients
P3H1	LIHC	Missense_Mutation	2	0.5%	373

B

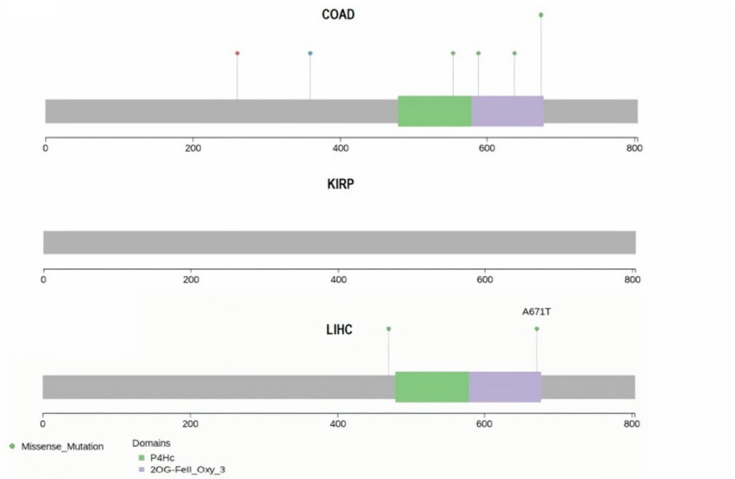

C

Significant probe highlighted (p<0.05)

Gene	Probe	Chr	Position	Average of Cancer Sample	Average of Normal Sample	p-value
P3H1	cg21389776	chr1	42746753	0.88	0.88	3.3e-01
P3H1	cg23287466	chr1	42750158	0.91	0.90	3.8e-01
P3H1	cg11856487	chr1	42754125	0.69	0.70	3.3e-02
P3H1	cg00917471	chr1	42762645	0.48	0.46	3.7e-01
P3H1	cg04118124	chr1	42765578	0.87	0.84	8.0e-02
P3H1	cg08116724	chr1	42765960	0.19	0.15	1.3e-07
P3H1	cg26337430	chr1	42766550	0.07	0.05	5.6e-07
P3H1	cg19044674	chr1	42766957	0.08	0.08	7.0e-01
P3H1	cg17973739	chr1	42766995	0.02	0.02	9.0e-01
P3H1	cg21881116	chr1	42767182	0.04	0.03	6.0e-02
P3H1	cg04342538	chr1	42767240	0.03	0.02	1.3e-01
P3H1	cg06802655	chr1	42767246	0.03	0.03	2.8e-01
P3H1	cg09501274	chr1	42767396	0.04	0.03	1.1e-01
P3H1	cg01724006	chr1	42767401	0.02	0.02	1.2e-04
P3H1	cg12108527	chr1	42767480	0.05	0.04	2.0e-03
P3H1	cg00451039	chr1	42767540	0.03	0.04	4.2e-01
P3H1	cg16822606	chr1	42767668	0.03	0.03	5.7e-02
P3H1	cg09348084	chr1	42767687	0.05	0.04	2.2e-05
P3H1	cg27657283	chr1	42767852	0.04	0.03	2.5e-02

Significant probe highlighted (p<0.05)

Gene	Probe	Chr	Position	Average of Cancer Sample	Average of Normal Sample	p-value
P3H1	cg21389776	chr1	42746753	0.89	0.91	4.0e-06
P3H1	cg23287466	chr1	42750158	0.91	0.92	3.6e-01
P3H1	cg11856487	chr1	42754125	0.63	0.68	8.8e-03
P3H1	cg00917471	chr1	42762645	0.58	0.78	0.0e+00
P3H1	cg04118124	chr1	42765578	0.52	0.37	2.2e-16
P3H1	cg08116724	chr1	42765960	0.09	0.08	8.0e-04
P3H1	cg26337430	chr1	42766550	0.05	0.05	9.1e-01
P3H1	cg19044674	chr1	42766957	0.08	0.07	7.2e-01
P3H1	cg17973739	chr1	42766995	0.01	0.01	3.2e-07
P3H1	cg21881116	chr1	42767182	0.03	0.03	2.7e-01
P3H1	cg04342538	chr1	42767240	0.02	0.02	2.9e-07
P3H1	cg06802655	chr1	42767246	0.03	0.02	4.2e-05
P3H1	cg09501274	chr1	42767396	0.03	0.02	1.8e-11
P3H1	cg01724006	chr1	42767401	0.01	0.01	1.9e-07
P3H1	cg12108527	chr1	42767480	0.04	0.04	1.0e-01
P3H1	cg00451039	chr1	42767540	0.35	0.03	0.0e+00
P3H1	cg16822606	chr1	42767668	0.03	0.03	5.2e-03
P3H1	cg09348084	chr1	42767687	0.05	0.04	1.2e-02
P3H1	cg27657283	chr1	42767852	0.03	0.03	8.0e-02

Significant probe highlighted (p<0.05)

Gene	Probe	Chr	Position	Average of Cancer Sample	Average of Normal Sample	p-value
P3H1	cg21389776	chr1	42746753	0.87	0.88	7.7e-02
P3H1	cg23287466	chr1	42750158	0.90	0.90	5.0e-01
P3H1	cg11856487	chr1	42754125	0.66	0.65	8.8e-01
P3H1	cg00917471	chr1	42762645	0.72	0.73	2.5e-01
P3H1	cg04118124	chr1	42765578	0.64	0.72	3.1e-08
P3H1	cg08116724	chr1	42765960	0.09	0.09	6.4e-01
P3H1	cg26337430	chr1	42766550	0.05	0.05	1.0e+00
P3H1	cg19044674	chr1	42766957	0.08	0.07	2.9e-01
P3H1	cg17973739	chr1	42766995	0.02	0.02	2.4e-01
P3H1	cg21881116	chr1	42767182	0.04	0.03	8.3e-05
P3H1	cg04342538	chr1	42767240	0.02	0.03	1.3e-01
P3H1	cg06802655	chr1	42767246	0.03	0.03	7.5e-02
P3H1	cg09501274	chr1	42767396	0.03	0.03	1.2e-01
P3H1	cg01724006	chr1	42767401	0.02	0.02	6.6e-01
P3H1	cg12108527	chr1	42767480	0.05	0.05	1.1e-02
P3H1	cg00451039	chr1	42767540	0.03	0.03	2.7e-01
P3H1	cg16822606	chr1	42767668	0.03	0.03	9.9e-01
P3H1	cg09348084	chr1	42767687	0.05	0.05	6.0e-02
P3H1	cg27657283	chr1	42767852	0.03	0.03	1.8e-01

D

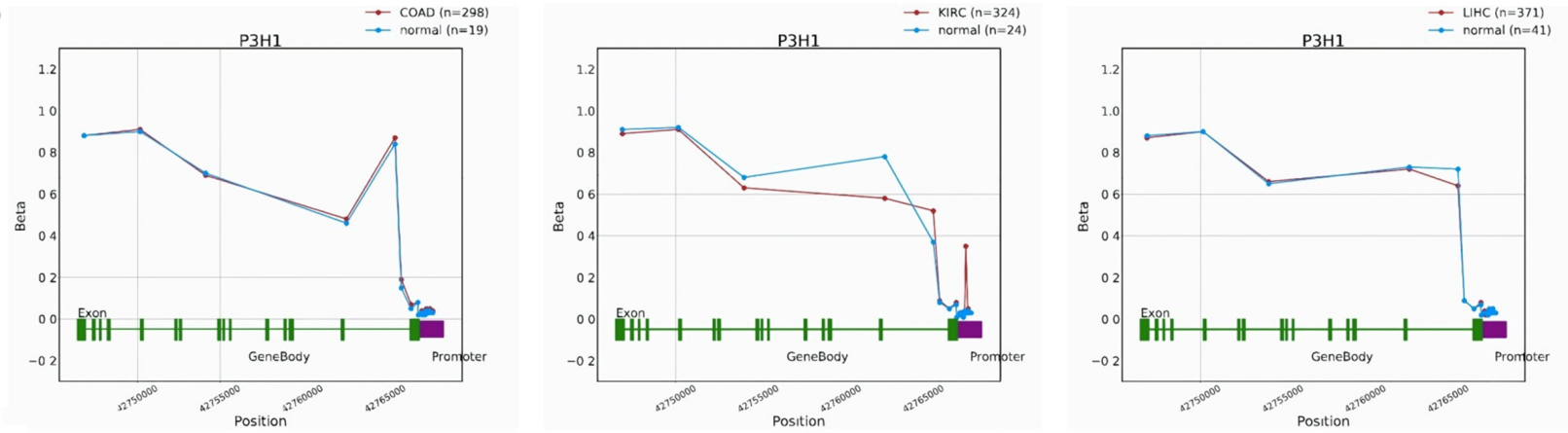

Figure 4. Mutation and promoter methylation analysis of Prolyl 3-Hydroxylase 1 (P3H1) across colon adenocarcinoma (COAD), kidney renal clear cell carcinoma (KIRC), and liver hepatocellular carcinoma (LIHC) using the OncoDB database. A. Mutation subtypes of P3H1 in colon adenocarcinoma (COAD), kidney renal papillary cell carcinoma (KIRP), and liver hepatocellular carcinoma (LIHC) based on combined DNA-seq and RNA-seq analyses. B. Visual representation of P3H1 mutation positions and their distribution across protein domains (P4Hc and 2OG-FeII_Oxy_3 domains) in COAD, KIRP, and LIHC. C. Significant methylation probes for P3H1 (highlighted in yellow) in COAD, KIRP, and LIHC cancer samples, comparing methylation levels between cancer and normal tissues. D. Methylation profile across the P3H1 gene body and promoter regions in COAD, KIRP, and LIHC cancer types, displaying beta values of significant probes. $P < 0.05$.

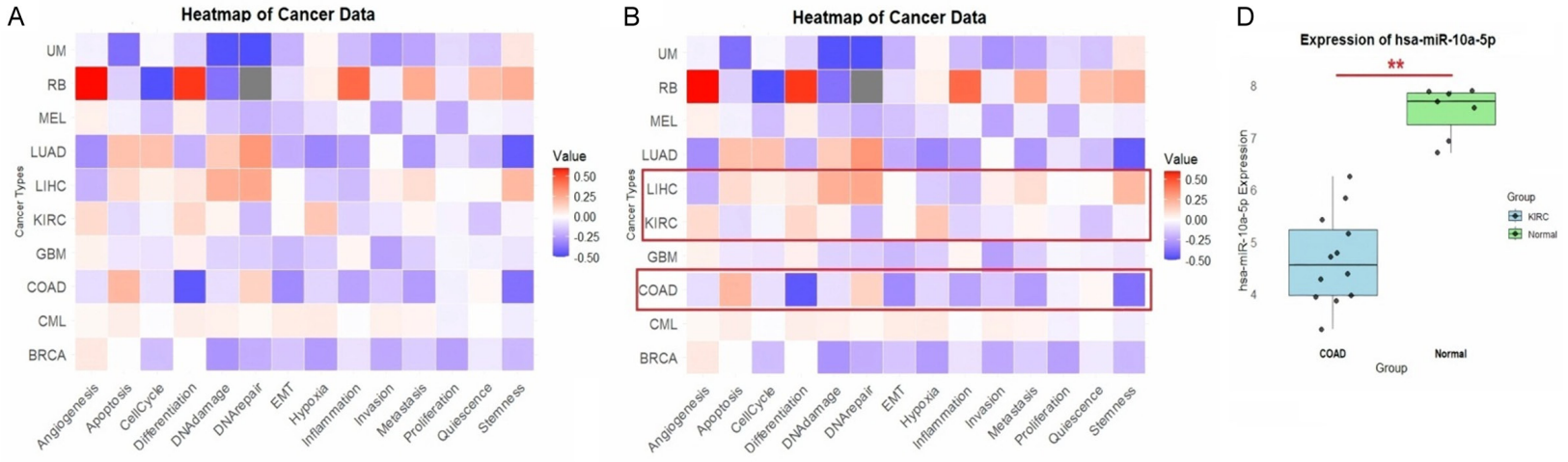

C

	Predicted consequential pairing of target region (top) and miRNA (bottom)	Site type	Context++ score	Context++ score percentile	Weighted context++ score	Conserved branch length	P_{CT}	Predicted relative K_D
Position 61-67 of LEPRE1 3' UTR hsa-miR-10b-5p	5' ...GUUUGUCCUUGCAGGACAGGGUG... 3' GUGUUUAAGCCAAGAUGUCCCAU	7mer-m8	-0.11	82	-0.11	2.841	N/A	-2.470
Position 61-67 of LEPRE1 3' UTR hsa-miR-10a-5p	5' ...GUUUGUCCUUGCAGGACAGGGUG... 3' GUGUUUAAGCCUAGAUGUCCCAU	7mer-m8	-0.11	82	-0.11	2.841	N/A	-2.470

Figure 5. Correlation of Prolyl 3-Hydroxylase 1 (P3H1) with functional states, MicroRNA (miRNA) prediction, and expression analysis. A. Heatmap showing the correlation of P3H1 with various functional states across different cancer, including colon adenocarcinoma (COAD), kidney renal clear cell carcinoma (KIRC), and liver hepatocellular carcinoma (LIHC) using the CancerSEA database. B. Heatmap specifically showing the correlation of P3H1 with various functional states across COAD, KIRC, and LIHC using the CancerSEA database. C. Predication and sequence alignment of the miRNA (hsa-miR-10a-5p) that regulates P3H1 expression using TargetScan database. D. Reverse Transcription Quantitative Polymerase Chain Reaction (RT-qPCR)-based expression analysis of the predicted miRNA (hsa-miR-10a-5p) in COAD and normal tissue samples. $^{**}P < 0.01$.

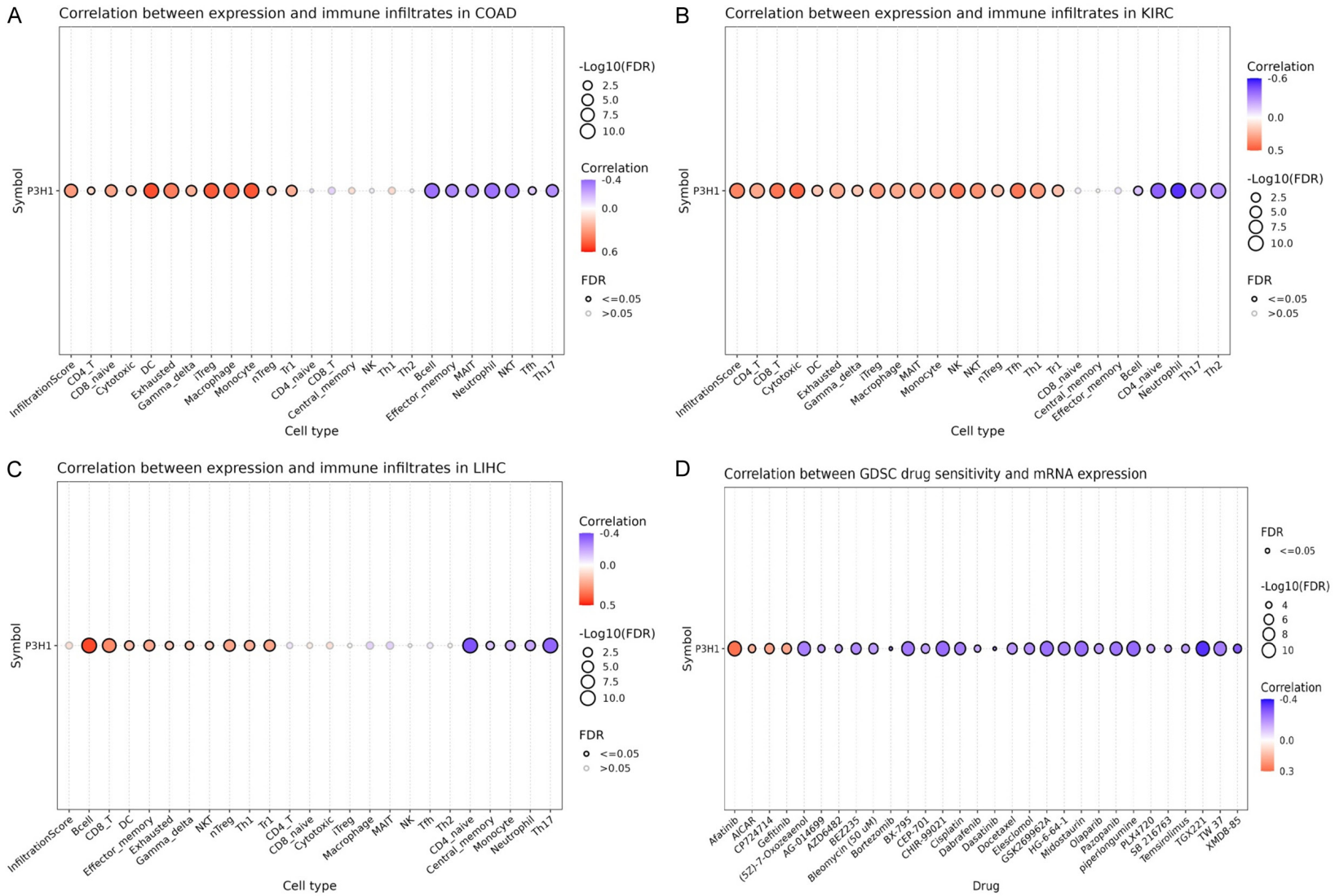

Figure 6. Correlation analysis of Prolyl 3-Hydroxylase 1 (P3H1) expression with immune infiltration and drug sensitivity in colon adenocarcinoma (COAD), kidney renal clear cell carcinoma (KIRC), and liver hepatocellular carcinoma (LIHC). A. Correlation between P3H1 expression and immune cell infiltration in COAD. B. Correlation between P3H1 expression and immune cell infiltration in KIRC. C. Correlation between P3H1 expression and immune cell infiltration in LIHC. D. Correlation between P3H1 mRNA expression and drug sensitivity in cancer cell lines from the Genomics of Drug Sensitivity in Cancer (GDSC) database. $P < 0.05$.

gesting that high P3H1 expression may influence the sensitivity of cancer cells to such treatment.

Gene enrichment analysis of PH3P1

The PPI network analysis of P3H1, constructed by the STRING database, reveals that P3H1 is part of a tightly connected cluster of proteins, including COL1A1, COL1A2, COL5A1, P4HB, SERPINH1, and others (**Figure 7A**). Gene enrichment analysis further clarified the biological significance of these interactions. In **Figure 7B**, cellular component (CC) enrichment analysis showed that the most enriched terms are associated with the endoplasmic reticulum chaperone complex, fibrillar collagen trimer, and the collagen-containing extracellular matrix. These terms point to P3H1's role in the endoplasmic reticulum, where it participates in post-translational modification and collagen formation. **Figure 7C** represents molecular function (MF) enrichment, and highlights significant enrichment for procollagen-proline 4-dioxygenase activity, peptidyl-proline hydroxylation, and collagen-binding activity. These functions are critical for hydroxylation of proline residues in collagen, a modification that is essential for the stability and functionality of collagen fibers. In **Figure 7D**, biological process (BP) enrichment analysis emphasizes that the P3H1-associated network is involved in processes such as the negative regulation of post-translational protein modification, peptidyl-proline hydroxylation, and collagen fibril organization. This suggests that P3H1 plays a key role in regulating the modification, assembly, and structural integrity of collagen in the extracellular matrix. Finally, **Figure 7E** shows pathway enrichment analysis, where key pathways like ECM-receptor interaction, AGE-RAGE signaling in diabetic complications, and the PI3K-Akt signaling pathway are significantly enriched. These pathways indicate that P3H1 and its associated proteins not only influence collagen structure and extracellular matrix remodeling but also participate in cellular adhesion, signaling, and potentially in disease mechanisms related to metabolism and inflammation, such as fibrosis, cancer, and diabetic complications.

Validation of P3H1 expression in the serum of COAD patients

ELISA was used to assess the P3H1 level in serum samples from the patients with COAD (n = 60) and healthy subjects (n = 30). The COAD group demonstrates a significantly (p-value < 0.001) higher serum concentration of P3H1 compared to the control group (**Figure 8A**). **Figure 8B** depicts a ROC curve, which evaluates the diagnostic efficacy of P3H1 in distinguishing between COAD patients and healthy controls. The curve shows the trade-off between sensitivity (true positive rate) and specificity (false positive rate), with the area under the curve (AUC) approaching 1.0 (**Figure 8B**). This near-perfect AUC suggests that P3H1 has excellent diagnostic accuracy for identifying COAD patients from the control group, and may be a reliable biomarker for the disease.

P3H1 knockdown and functional assays

The effects of P3H1 knockdown on the proliferation, colony formation, and migratory abilities of HCT116 cells were analyzed to evaluate the biological significance of P3H1 in COAD. After P3H1 knockdown, its expression was assessed to confirm the knockdown efficiency of P3H1-specific siRNA (si-P3H1). **Figure 9A** indicated a significant reduction in P3H1 mRNA levels in si-P3H1-treated cells compared to control cells (Ctrl-HCT116), validating the effectiveness of the knockdown approach (**Figure 9A**). **Figure 9B** presents cell proliferation assay results, which revealed that silencing P3H1 results in a marked decrease in cell proliferation rates of si-P3H1 cells compared to the Ctrl-HCT116 cells (**Figure 9B**). In **Figure 9C** and **9D**, colony formation capacity - a measure of long-term cell survival and anchorage-independent growth - was assessed. Representative images and quantification indicated a substantial reduction in colony numbers in the si-P3H1 cells compared to the Ctrl-HCT116 cells (**Figure 9C**, **9D**). Finally, the wound healing assay, displayed in **Figure 9E-G**, showed the effect of P3H1 knockdown on cell migration. Compared to Ctrl-HCT116 cells, the si-P3H1-treated cells exhibit slower wound closure over 24 hours, as depicted in the wound closure images (**Figure 9F**). Collectively, these findings indicate that P3H1 knockdown impairs cell proliferation, colony formation, and migration in HCT116 cells, highlighting P3H1 as a potential oncogenic factor in COAD progression.

Discussion

Cancer is a leading cause of morbidity and mortality worldwide, characterized by uncontrolled

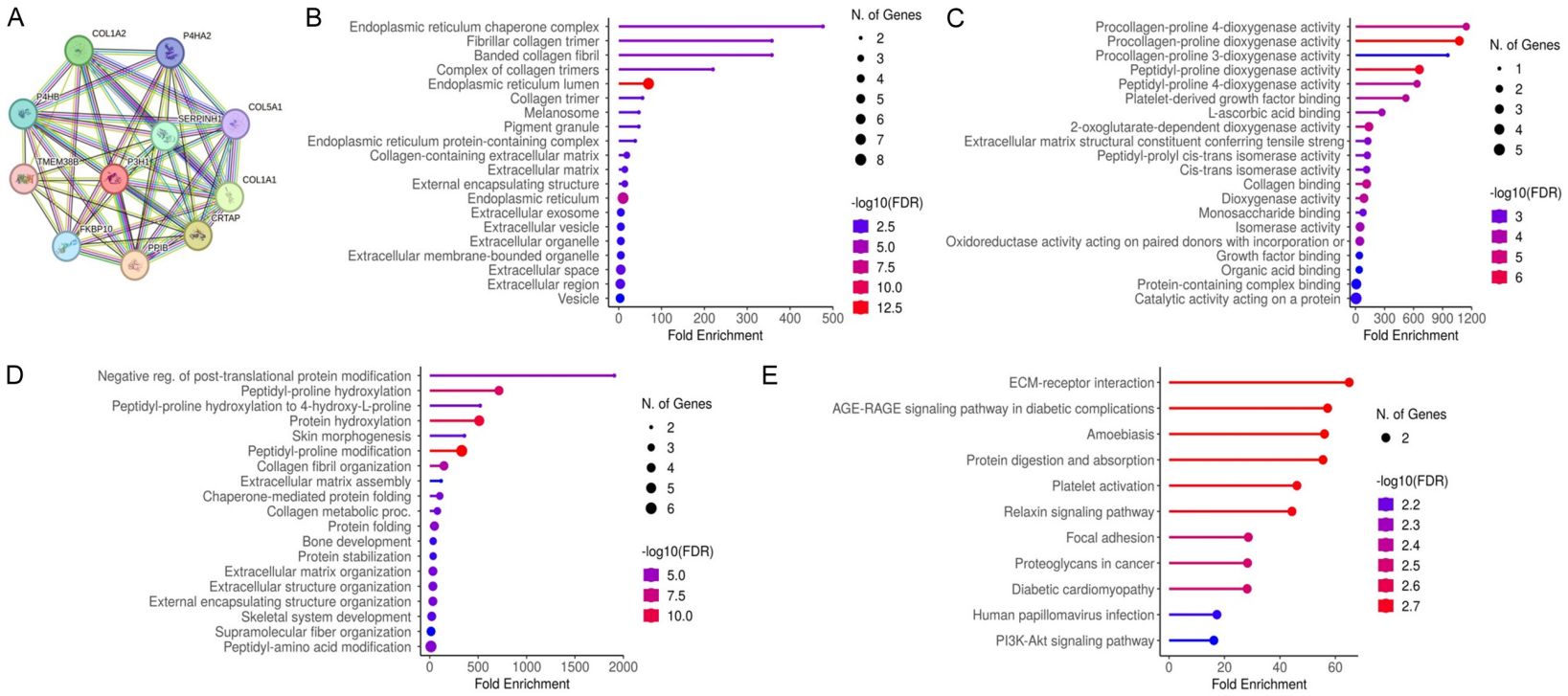

Figure 7. Protein-protein interaction (PPI) network and gene enrichment analysis of Prolyl 3-Hydroxylase 1 (P3H1)-associated genes. A. PPI network of P3H1 and its interacting proteins, constructed using the STRING database. B. Gene Ontology (GO) enrichment analysis for cellular component categories. C. GO enrichment analysis for molecular function categories. D. GO enrichment analysis for biological process categories. E. Kyoto Encyclopedia of Genes and Genomes (KEGG) pathway enrichment analysis of genes in the PPI network. $P < 0.05$.

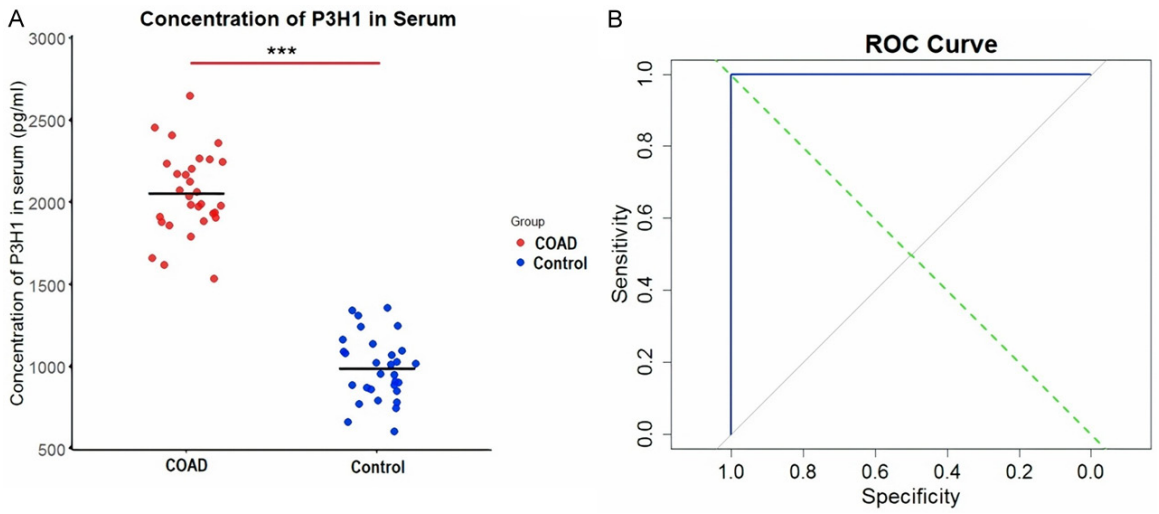

Figure 8. Prolyl 3-Hydroxylase 1 (P3H1) serum levels in healthy individuals and colorectal adenocarcinoma (COAD) patients. A. P3H1 levels in the serum of COAD patients (n = 60) and healthy controls (n = 30) were measured using enzyme linked immunosorbent assay. B. The area under the curve (AUC) reached 1.00. ***P < 0.001.

cell proliferation and ability to invade other tissues [37, 38]. With over 18 million new cases diagnosed globally in 2023, cancer's burden is rising, necessitating urgent advancement in prevention, detection, and treatment strategies [39]. The complexity of cancer biology is further compounded by its heterogeneity, both within and between tumor types [40, 41]. This diversity leads to variable patient outcomes, underscoring the need for tailored therapeutic approaches. Traditionally, cancer research has focused on individual types of malignancy, limiting our understanding of common mechanisms that underlie tumorigenesis [41]. Recent advances in genomics and bioinformatics have facilitated the exploration of shared molecular signatures across various cancers, revealing therapeutic targets and biomarkers that transcend specific cancer types [42, 43]. This pan-cancer analysis allows researchers to identify key players in tumor biology that may serve as universal biomarkers for diagnosis and prognosis. The increasing understanding of the shared molecular pathways across different cancers necessitates a pan-cancer analysis approach [44]. Pan-cancer studies can uncover global trends in tumor biology, reveal genetic and epigenetic alterations common to multiple cancer types, and identify therapeutic targets that may improve treatment efficacy across diverse patient populations [45, 46]. Moreover, such studies enhance our understanding of cancer biology and provide insight into how tumor microenvironments may differ based on tissue of origin, which can influence treatment response [46].

In this study, we analyzed P3H1 expression across multiple human cancers using comprehensive methodology. Our analysis indicated a substantial increase in P3H1 mRNA and protein levels in several cancer types. This widespread upregulation of P3H1 in various cancers supports the hypothesis that it may play a role in tumorigenesis or tumor progression.

Notably, our findings align with previous studies that have reported elevated P3H1 expression in BRCA and LUAD. For instance, Shah et al. demonstrated that P3H1 enhances tumor growth and metastasis in BRCA [23], possibly through its role in collagen synthesis and modulation of the extracellular matrix (ECM). Similarly, a study by Wu et al., in LUAD indicated that P3H1 contributes to the aggressive behavior of tumors through the regulation of collagen deposition and tumor microenvironment modulation [24]. However, the absence of significant P3H1 expression alterations in certain cancer types (e.g., CESC, PAAD, PCPG, and SKCM) highlights the need for context-specific analyses, as the biological roles of genes can differ significantly depending on the cancer type.

Furthermore, the prognostic significance of P3H1 was assessed using Kaplan-Meier survival analyses, revealing that high P3H1 expres-

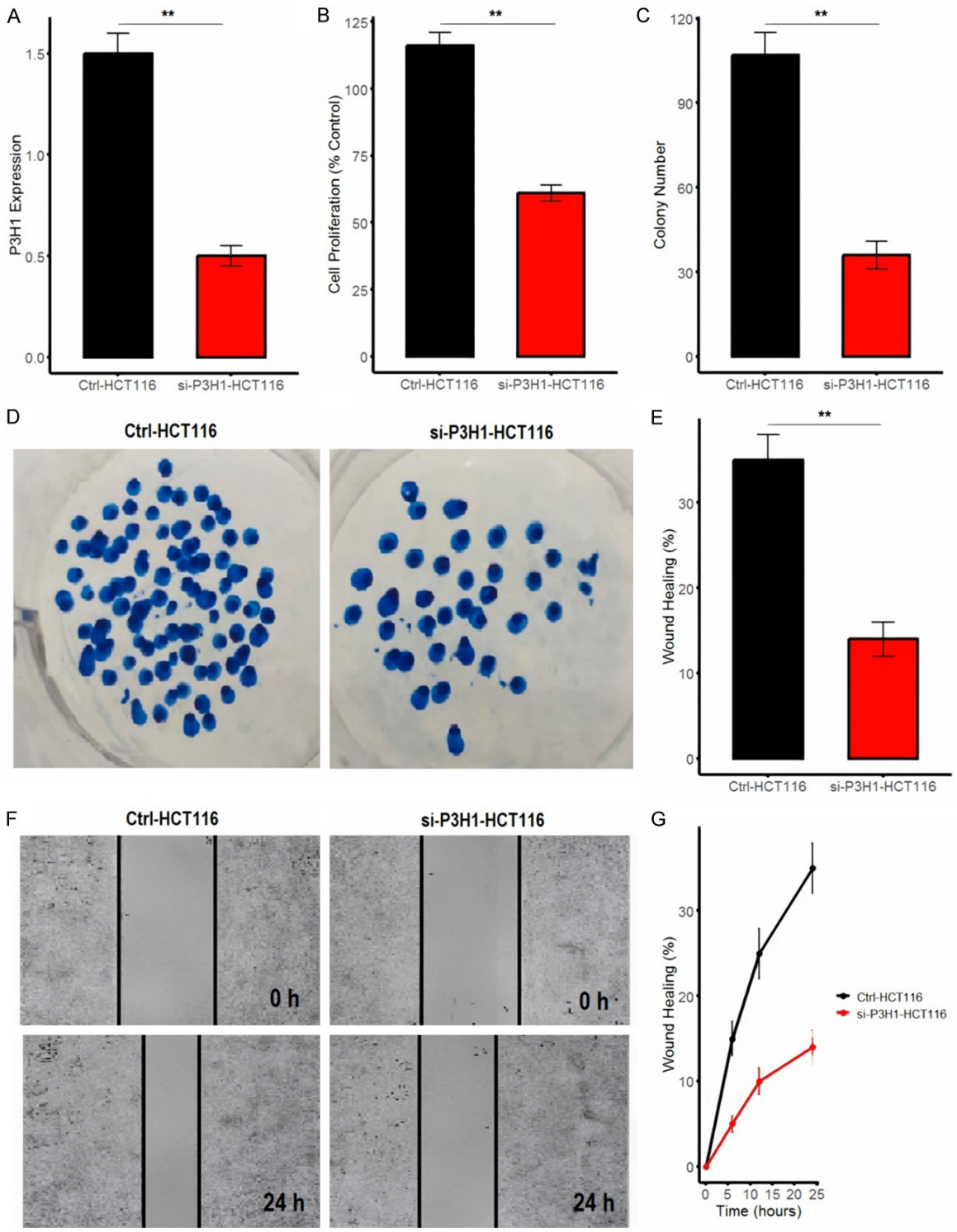

Figure 9. Knockdown of Prolyl 3-Hydroxylase 1 (P3H1) inhibits proliferation, colony formation, and migration in HCT116 cells. A. Reverse transcription quantitative polymerase chain reaction (RT-qPCR) analysis of P3H1 mRNA levels in control (Ctrl-HCT116) and P3H1 knockdown (si-P3H1-HCT116) cells, confirming successful knockdown. B. Cell proliferation assay showed a significant decrease in proliferation rates in si-P3H1-HCT116 cells compared to control cells. C. Quantification of colony numbers. D. Colony formation assay with representative images. E. P3H1 knockdown resulted in significantly slower wound closure, indicating reduced migratory ability in si-P3H1-HCT116 cells compared to control. F. Quantification of wound healing percentage. G. A time-course analysis of wound healing. **P < 0.01.

sion correlates with poorer survival outcomes in COAD, KIRC, and LIHC. These findings are consistent with previous literature indicating that elevated P3H1 levels are associated with adverse prognoses in various cancers. For instance, Li et al. found that high P3H1 expression correlates with worse overall survival in BRCA [47], supporting our results in LIHC. The mechanism by which P3H1 influences cancer prognosis may involve its role in ECM remodeling. As a prolyl 4-hydroxylase, P3H1 is crucial for collagen modification, impacting tumor stiffness and extracellular matrix integrity. Studies have shown that alterations in collagen architecture can facilitate tumor invasion and metastasis, thereby influencing patient survival [48, 49]. This suggests that P3H1 may serve as both a biomarker for poor prognosis and a therapeutic target for modulating ECM dynamics in cancer.

Our investigation into the correlation between P3H1 expression and clinical variables further elucidates its possible role in cancer biology. We observed significant upregulation of P3H1 in COAD across all stages compared to normal tissues, indicating that P3H1 expression may correlate with disease progression. This finding aligns with previous reports that have demonstrated a gradual increase in P3H1 expression corresponding to tumor advancement [17, 50]. Further analysis of genetic mutations and promoter methylation of P3H1 revealed low mutation frequencies in COAD, KIRC, and LIHC, suggesting that P3H1 expression is primarily regulated at the transcriptional level rather than through mutations. The differential methylation patterns observed in COAD and KIRC, with lower methylation levels in cancer samples compared to normal tissues, suggest a mechanism of upregulation through hypomethylation. These findings are supported by previous studies that have reported similar patterns of promoter hypomethylation leading to increased gene expression in various cancers. For instance, a study by Zolota et al., reported that hypomethylation of genes involved in ECM remodeling can lead to increased tumor aggressiveness [51]. However, the lack of significant methylation differences in LIHC indicates that alternative regulatory mechanisms may govern P3H1 expression in this cancer type. The findings of this study also demonstrate that P3H1 expression negatively correlates with the infiltration of specific immune cell types in COAD, KIRC, and LIHC. This suggests that higher P3H1 levels may contribute to an immunosuppressive tumor microenvironment, which could facilitate tumor progression and resistance to therapy. Previous research has identified similar trends, with certain proteins linked to immune evasion in various cancers [52, 53].

The pathway enrichment analysis emphasizes the crucial role of P3H1 in significant cancer-related pathways, including ECM-receptor interaction and PI3K-Akt signaling. These pathways are essential for regulating various cellular processes, such as tumor growth, metastasis, and treatment resistance, which are pivotal in the progression of cancer. The ECM-receptor interaction pathway is particularly important as it facilitates communication between tumor cells and the extracellular matrix, influencing cellular behavior and metastatic potential [54]. Similarly, the PI3K-Akt signaling pathway is well-known for its role in cell survival, proliferation, and metabolism, making it a key player in cancer cell dynamics [55]. Given the involvement of P3H1 in these pathways, targeting P3H1 could offer promising therapeutic benefits for cancer management.

This study presents several strengths and limitations regarding the role of P3H1 in cancer. One of its main strengths is the comprehensive pan-cancer analysis utilizing robust datasets like TCGA, which allows for reliable cross-validation of results. The research effectively links P3H1 expression with patient survival outcome and clinical variables, enhancing the clinical relevance of its findings. Additionally, the investigation of molecular mechanisms, such as immune infiltration and miRNA regulation, offers insight into cancer progression and treatment response. However, there are limitations, including the influence of confounding factors and the lack of longitudinal data, which may restrict the interpretations of the results. Addressing these limitations in future studies will be essential for deepening the understanding of P3H1 as a biomarker or therapeutic target.

Conclusion

This study highlights the significant role of P3H1 in various human cancers, particularly COAD, KIRC, and LIHC. The comprehensive

analysis demonstrates that P3H1 expression is upregulated in multiple cancer types, correlating with poor prognosis and adverse clinical variables. The investigation into genetic mutations and promoter methylation reveals low mutation frequencies, suggesting that P3H1 dysregulation may primarily stem from epigenetic mechanisms rather than genetic alterations. Furthermore, the study uncovers critical relationships between P3H1 expression and immune cell infiltration, indicating an impact on the tumor microenvironment and immune response. The validation of P3H1 as a diagnostic biomarker in COAD patients, evidenced by significantly elevated serum levels, emphasizes its potential utility in clinical settings. Overall, these findings pave the way for further exploration of P3H1 as a therapeutic target and biomarker in cancer management. Additional studies will elucidate its functional mechanisms and interactions within the tumor landscape.

Acknowledgements

The authors extend their appreciation to the Researchers Supporting Project number (RSPD2025R552) King Saud University, Riyadh, Saud Arabia.

Disclosure of conflict of interest

None.

Abbreviations

ACC, Adrenocortical Carcinoma; BLCA, Bladder Urothelial Carcinoma; BRCA, Breast Invasive Carcinoma; CESC, Cervical Squamous Cell Carcinoma and Endocervical Adenocarcinoma; CHOL, Cholangiocarcinoma; COAD, Colon Adenocarcinoma; DLBC, Lymphoid Neoplasm Diffuse Large B-cell Lymphoma; ESCA, Esophageal Carcinoma; GBM, Glioblastoma Multiforme; HNSC, Head and Neck Squamous Cell Carcinoma; KICH, Kidney Chromophobe; KIRC, Kidney Renal Clear Cell Carcinoma; KIRP, Kidney Renal Papillary Cell Carcinoma; LAMAL, Acute Myeloid Leukemia; LGG, Low-Grade gGioma; LIHC, Liver Hepatocellular Carcinoma; LUAD, Lung Adenocarcinoma; LUSC, Lung Squamous Cell Carcinoma; MESO, Mesothelioma; OV, Ovarian Serous Cystadenocarcinoma; PAAD, Pancreatic Adenocarcinoma; PCPG, Pheochromocytoma and Paraganglioma; PRAD, Prostate Adenocarcinoma; READ, Rectum Adenocarcinoma; SARC, Sarcoma; SKCM, Skin Cutaneous Melanoma; STAD, Stomach Adenocarcinoma; TGCT, Testicular Germ Cell Tumors; THCA, Thyroid Carcinoma; THYM, Thymoma; UCEC, Uterine Corpus Endometrial Carcinoma; UCS, Uterine Carcinosarcoma; UVM, Uveal Melanoma; LEPRE1, Leprecan-like Protein 1; TCGA, The Cancer Genome Atlas; CPTAC, Clinical Proteomic Tumor Analysis Consortium; TPM, Transcripts Per Million.

Address correspondence to: Mostafa A Abdel-Maksoud, Department of Botany and Microbiology, College of Science, King Saud University, Riyadh 11451, Saudi Arabia. E-mail: mabdmaksoud@ksu.edu.sa

References

[1] Ghufran MS, Soni P and Duddukuri GR. The global concern for cancer emergence and its prevention: a systematic unveiling of the present scenario. Bioprospecting of Tropical Medicinal Plants. Springer; 2023. pp. 1429-1455.

[2] Li L, Shan T, Zhang D and Ma F. Nowcasting and forecasting global aging and cancer burden: analysis of data from the GLOBOCAN and Global Burden of Disease Study. J Natl Cancer Cent 2024; 4: 223-232.

[3] Abdel-Maksoud MA, Ullah S, Nadeem A, Shaikh A, Zia MK, Zakri AM, Almanaa TN, Alfuraydi AA, Mubarak A and Hameed Y. Unlocking the diagnostic, prognostic roles, and immune implications of BAX gene expression in pan-cancer analysis. Am J Transl Res 2024; 16: 63-74.

[4] Dong Y, Wu X, Xu C, Hameed Y, Abdel-Maksoud MA, Almanaa TN, Kotob MH, Al-Qahtani WH, Mahmoud AM, Cho WC and Li C. Prognostic model development and molecular subtypes identification in bladder urothelial cancer by oxidative stress signatures. Aging (Albany NY) 2024; 16: 2591-2616.

[5] Zhang S, Jin Z, Bao L and Shu P. The global burden of breast cancer in women from 1990 to 2030: assessment and projection based on the global burden of disease study 2019. Front Oncol 2024; 14: 1364397.

[6] Siegel RL, Giaquinto AN and Jemal A. Cancer statistics, 2024. CA Cancer J Clin 2024; 74: 12-49.

[7] Xia C, Dong X, Li H, Cao M, Sun D, He S, Yang F, Yan X, Zhang S, Li N and Chen W. Cancer statistics in China and United States, 2022: profiles, trends, and determinants. Chin Med J (Engl) 2022; 135: 584-590.

[8] Hu H, Umair M, Khan SA, Sani AI, Iqbal S, Khalid F, Sultan R, Abdel-Maksoud MA, Mubarak A, Dawoud TM, Malik A, Saleh IA, Al

Amri AA, Algarzae NK, Kodous AS and Hameed Y. CDCA8, a mitosis-related gene, as a prospective pan-cancer biomarker: implications for survival prognosis and oncogenic immunology. Am J Transl Res 2024; 16: 432-445.
[9] Hameed Y and Ejaz S. TP53 lacks tetramerization and N-terminal domains due to novel inactivating mutations detected in leukemia patients. J Cancer Res Ther 2021; 17: 931-937.
[10] Ahmad M, Khan M, Asif R, Sial N, Abid U, Shamim T, Hameed Z, Iqbal MJ, Sarfraz U and Saeed H. Expression characteristics and significant diagnostic and prognostic values of ANLN in human cancers. Int J Gen Med 2022; 1957-1972.
[11] Pulumati A, Pulumati A, Dwarakanath BS, Verma A and Papineni RVL. Technological advancements in cancer diagnostics: improvements and limitations. Cancer Rep (Hoboken) 2023; 6: e1764.
[12] Tavares V, Marques IS, Melo IG, Assis J, Pereira D and Medeiros R. Paradigm shift: a comprehensive review of ovarian cancer management in an era of advancements. Int J Mol Sci 2024; 25: 1845.
[13] Ullah L, Hameed Y, Ejaz S, Raashid A, Iqbal J, Ullah I and Ejaz SA. Detection of novel infiltrating ductal carcinoma-associated BReast CAncer gene 2 mutations which alter the deoxyribonucleic acid-binding ability of BReast CAncer gene 2 protein. J Cancer Res Ther 2020; 16: 1402-1407.
[14] Wang Y, Wu Q, Liu J, Wang X, Xie J, Fu X and Li Y. WDR77 in pan-cancer: revealing expression patterns, genetic insights, and functional roles across diverse tumor types, with a spotlight on colorectal cancer. Transl Oncol 2024; 49: 102089.
[15] Lin Y, Xiong Z, Yang Y, Li W, Huang W, Lin M and Zhang S. Pan-cancer bioinformatics analysis of hepatic leukemia factor and further validation in colorectal cancer. Transl Cancer Res 2024; 13: 3299-3317.
[16] Li K, Guo C, Li R, Yao Y, Qiang M, Chen Y, Tu K and Xu Y. Pan-cancer characterization of cellular senescence reveals its inter-tumor heterogeneity associated with the tumor microenvironment and prognosis. Comput Biol Med 2024; 182: 109196.
[17] Pignata P, Apicella I, Cicatiello V, Puglisi C, Magliacane Trotta S, Sanges R, Tarallo V and De Falco S. Prolyl 3-hydroxylase 2 is a molecular player of angiogenesis. Int J Mol Sci 2021; 22: 3896.
[18] Li W, Peng J, Yao D, Rao B, Xia Y, Wang Q, Li S, Cao M, Shen Y, Ma P, Liao R, Qin A, Zhao J and Cao Y. The structural basis for the collagen processing by human P3H1/CRTAP/PPIB ternary complex. Nat Commun 2024; 15: 7844.
[19] Prakash J and Shaked Y. The interplay between extracellular matrix remodeling and cancer therapeutics. Cancer Discov 2024; 14: 1375-1388.
[20] Mancini A, Gentile MT, Pentimalli F, Cortellino S, Grieco M and Giordano A. Multiple aspects of matrix stiffness in cancer progression. Front Oncol 2024; 14: 1406644.
[21] van Haaften WT, Blokzijl T, Hofker HS, Olinga P, Dijkstra G, Bank RA and Boersema M. Intestinal stenosis in Crohn's disease shows a generalized upregulation of genes involved in collagen metabolism and recognition that could serve as novel anti-fibrotic drug targets. Therap Adv Gastroenterol 2020; 13: 1756284820952578.
[22] Deng F, Zhou K, Li Q, Liu D, Li M, Wang H, Zhang W and Ma Y. iTRAQ-based quantitative proteomic analysis of esophageal squamous cell carcinoma. Tumour Biol 2016; 37: 1909-1918.
[23] Shah R, Smith P, Purdie C, Quinlan P, Baker L, Aman P, Thompson AM and Crook T. The prolyl 3-hydroxylases P3H2 and P3H3 are novel targets for epigenetic silencing in breast cancer. Br J Cancer 2009; 100: 1687-1696.
[24] Zhang Y, Chen Y, Chen Z, Zhou X, Chen S, Lan K and Zhang Y. Identification of P3H1 as a predictive prognostic biomarker for bladder urothelial carcinoma based on the cancer genome atlas database. Pharmgenomics Pers Med 2023; 16: 1041-1053.
[25] Li Y, Chen Y, Ma Y, Nenkov M, Haase D and Petersen I. Collagen prolyl hydroxylase 3 has a tumor suppressive activity in human lung cancer. Exp Cell Res 2018; 363: 121-128.
[26] Wang Z and Wang H. The role of P3H family in cancer: implications for prognosis, tumor microenvironment and drug sensitivity. Front Oncol 2024; 14: 1374696.
[27] Li T, Fu J, Zeng Z, Cohen D, Li J, Chen Q, Li B and Liu XS. TIMER2.0 for analysis of tumor-infiltrating immune cells. Nucleic Acids Res 2020; 48: W509-W514.
[28] Chandrashekar DS, Karthikeyan SK, Korla PK, Patel H, Shovon AR, Athar M, Netto GJ, Qin ZS, Kumar S, Manne U, Creighton CJ and Varambally S. UALCAN: an update to the integrated cancer data analysis platform. Neoplasia 2022; 25: 18-27.
[29] Tang Z, Kang B, Li C, Chen T and Zhang Z. GEPIA2: an enhanced web server for large-scale expression profiling and interactive analysis. Nucleic Acids Res 2019; 47: W556-W560.
[30] Lánczky A and Győrffy B. Web-based survival analysis tool tailored for medical research (KMplot): development and implementation. J Med Internet Res 2021; 23: e27633.

[31] Tang G, Cho M and Wang X. OncoDB: an interactive online database for analysis of gene expression and viral infection in cancer. Nucleic Acids Res 2022; 50: D1334-D1339.
[32] Yuan H, Yan M, Zhang G, Liu W, Deng C, Liao G, Xu L, Luo T, Yan H, Long Z, Shi A, Zhao T, Xiao Y and Li X. CancerSEA: a cancer single-cell state atlas. Nucleic Acids Res 2019; 47: D900-D908.
[33] Agarwal V, Bell GW, Nam JW and Bartel DP. Predicting effective microRNA target sites in mammalian mRNAs. Elife 2015; 4: e05005.
[34] Liu CJ, Hu FF, Xie GY, Miao YR, Li XW, Zeng Y and Guo AY. GSCA: an integrated platform for gene set cancer analysis at genomic, pharmacogenomic and immunogenomic levels. Brief Bioinform 2023; 24: bbac558.
[35] Szklarczyk D, Gable AL, Lyon D, Junge A, Wyder S, Huerta-Cepas J, Simonovic M, Doncheva NT, Morris JH, Bork P, Jensen LJ and Mering CV. STRING v11: protein-protein association networks with increased coverage, supporting functional discovery in genome-wide experimental datasets. Nucleic Acids Res 2019; 47: D607-D613.
[36] Sherman BT, Hao M, Qiu J, Jiao X, Baseler MW, Lane HC, Imamichi T and Chang W. DAVID: a web server for functional enrichment analysis and functional annotation of gene lists (2021 update). Nucleic Acids Res 2022; 50: W216-W221.
[37] Mazingi D and Lakhoo K. Cancer development and progression and the "Hallmarks of Cancer". Pediatric Surgical Oncology. Springer; 2023. pp. 1-15.
[38] Starska-Kowarska K. The role of different immunocompetent cell populations in the pathogenesis of head and neck cancer-regulatory mechanisms of pro- and anti-cancer activity and their impact on immunotherapy. Cancers (Basel) 2023; 15: 1642.
[39] Devarbhavi H, Asrani SK, Arab JP, Nartey YA, Pose E and Kamath PS. Global burden of liver disease: 2023 update. J Hepatol 2023; 79: 516-537.
[40] Ottaiano A, Ianniello M, Santorsola M, Ruggiero R, Sirica R, Sabbatino F, Perri F, Cascella M, Di Marzo M, Berretta M, Caraglia M, Nasti G and Savarese G. From chaos to opportunity: decoding cancer heterogeneity for enhanced treatment strategies. Biology (Basel) 2023; 12: 1183.
[41] Gambardella V, Tarazona N, Cejalvo JM, Lombardi P, Huerta M, Roselló S, Fleitas T, Roda D and Cervantes A. Personalized medicine: recent progress in cancer therapy. Cancers (Basel) 2020; 12: 1009.
[42] Chen F, Zhang Y, Gibbons DL, Deneen B, Kwiatkowski DJ, Ittmann M and Creighton CJ. Pan-cancer molecular classes transcending tumor lineage across 32 cancer types, multiple data platforms, and over 10,000 cases. Clin Cancer Res 2018; 24: 2182-2193.
[43] Freed DM, Sommer J and Punturi N. Emerging target discovery and drug repurposing opportunities in chordoma. Front Oncol 2022; 12: 1009193.
[44] Li Y, Dou Y, Da Veiga Leprevost F, Geffen Y, Calinawan AP, Aguet F, Akiyama Y, Anand S, Birger C, Cao S, Chaudhary R, Chilappagari P, Cieslik M, Colaprico A, Zhou DC, Day C, Domagalski MJ, Esai Selvan M, Fenyö D, Foltz SM, Francis A, Gonzalez-Robles T, Gümüş ZH, Heiman D, Holck M, Hong R, Hu Y, Jaehnig EJ, Ji J, Jiang W, Katsnelson L, Ketchum KA, Klein RJ, Lei JT, Liang WW, Liao Y, Lindgren CM, Ma W, Ma L, MacCoss MJ, Martins Rodrigues F, McKerrow W, Nguyen N, Oldroyd R, Pilozzi A, Pugliese P, Reva B, Rudnick P, Ruggles KV, Rykunov D, Savage SR, Schnaubelt M, Schraink T, Shi Z, Singhal D, Song X, Storrs E, Terekhanova NV, Thangudu RR, Thiagarajan M, Wang LB, Wang JM, Wang Y, Wen B, Wu Y, Wyczalkowski MA, Xin Y, Yao L, Yi X, Zhang H, Zhang Q, Zuhl M, Getz G, Ding L, Nesvizhskii AI, Wang P, Robles AI, Zhang B and Payne SH; Clinical Proteomic Tumor Analysis Consortium. Proteogenomic data and resources for pan-cancer analysis. Cancer Cell 2023; 41: 1397-1406.
[45] De Matos MR, Posa I, Carvalho FS, Morais VA, Grosso AR and de Almeida SF. A systematic pan-cancer analysis of genetic heterogeneity reveals associations with epigenetic modifiers. Cancers (Basel) 2019; 11: 391.
[46] Witte T, Plass C and Gerhauser C. Pan-cancer patterns of DNA methylation. Genome Med 2014; 6: 66.
[47] Li C, Zhang L, Xu Y, Chai D, Nan S, Qiu Z, Wang W and Deng W. The prognostic significance and potential mechanism of prolyl 3-hydroxylase 1 in hepatocellular carcinoma. J Oncol 2022; 2022: 7854297.
[48] Yuan Z, Li Y, Zhang S, Wang X, Dou H, Yu X, Zhang Z, Yang S and Xiao M. Extracellular matrix remodeling in tumor progression and immune escape: from mechanisms to treatments. Mol Cancer 2023; 22: 48.
[49] Xu S, Xu H, Wang W, Li S, Li H, Li T, Zhang W, Yu X and Liu L. The role of collagen in cancer: from bench to bedside. J Transl Med 2019; 17: 309.
[50] Yang Y, Feng H, Tang Y, Wang Z, Qiu P, Huang X, Chang L, Zhang J, Chen YE, Mizrak D and Yang B. Bioengineered vascular grafts with a pathogenic TGFBR1 variant model aneurysm formation in vivo and reveal underlying collagen defects. Sci Transl Med 2024; 16: eadg6298.
[51] Zolota V, Tzelepi V, Piperigkou Z, Kourea H, Papakonstantinou E, Argentou MI and Karamanos NK. Epigenetic alterations in triple-negative breast cancer-the critical role of extracellular matrix. Cancers (Basel) 2021; 13: 713.

[52] Bintintan V, Burz C, Pintea I, Muntean A, Deleanu D, Lupan I and Samasca G. The importance of extracellular vesicle screening in gastric cancer: a 2024 update. Cancers (Basel) 2024; 16: 2574.
[53] Gourmet L, Sottoriva A, Walker-Samuel S, Secrier M and Zapata L. Immune evasion impacts the landscape of driver genes during cancer evolution. Genome Biol 2024; 25: 168.
[54] Pickup MW, Mouw JK and Weaver VM. The extracellular matrix modulates the hallmarks of cancer. EMBO Rep 2014; 15: 1243-1253.
[55] Morgos DT, Stefani C, Miricescu D, Greabu M, Stanciu S, Nica S, Stanescu-Spinu II, Balan DG, Balcangiu-Stroescu AE, Coculescu EC, Georgescu DE and Nica RI. Targeting PI3K/AKT/mTOR and MAPK signaling pathways in gastric cancer. Int J Mol Sci 2024; 25: 1848.